COMMUNICATION

Metal–organic polyhedra crosslinked supramolecular polymeric elastomers†

Jun Zhao, [iD] Lin Cheng, Kai Liu, Zhaoming Zhang, Wei Yu and Xuzhou Yan [iD] *

Herein, supramolecular polymeric elastomers crosslinked by metal–organic polyhedra (ElastoMOPs) were designed and developed as a novel hybrid system featuring not only tunable mechanical properties but also dynamic actuation behaviors in response to dichloromethane vapor.

Supramolecular architectures are ubiquitous in living organisms, and not only endow them with structural complexity and functional diversities but also make them dynamic and adaptive.[1] Inspired by natural species, artificial supramolecular assemblies such as mechanically interlocked molecules,[2] metal-coordination complexes,[3] and hydrogen-bonding based foldamers[4] are oftentimes employed to construct smart polymeric materials with self-healing,[5] stimuli-responsive,[6] and/or mechanically adaptive properties.[7] Among these modular structural motifs, supramolecular coordination complexes (SCCs) constructed by coordination-driven self-assembly have received intense interest in supramolecular chemistry and materials science. So far, various discrete two-dimensional (2D) metal–organic polygons or three-dimensional (3D) metal–organic polyhedra (MOPs) with elegant and precise geometries have been developed for many applications.[8] The facile modification of versatile functional groups on the peripheries of the MOPs makes them promising candidates as crosslinkers in the polymeric matrix to tune mechanical properties of materials.[9] At the same time, well-defined cavities have the potential to endow the resultant materials with additional functionalities including inclusion, recognition, separation, *etc.*[10] Therefore, metal–organic polygons or polyhedra are emerging as attractive entities for the fabrication of smart supramolecular polymeric materials.

Recent investigations have demonstrated the advantages of the incorporation of metal–organic polygons[11] or polyhedra[12] into supramolecular polymeric materials. For example, orthogonal

self-assembly driven by metal–ligand coordination of the metal–organic polygons and other noncovalent interactions such as H-bonding and host–guest interactions has resulted in hierarchical superstructures with emergent functions which are difficult to obtain by conventional covalent approaches.[9a,13] In addition to 2D metal–organic polygons, the hybridization of robust 3D metal–organic polyhedra and flexible polymers afforded stimuli-responsive and topology-switchable cavity-core supramolecular gels, which represent a new class of soft materials.[14] Furthermore, MOPs can also be used as monomers to participate in polymerization for the preparation of MOP-hybridized membranes with inherent characteristics such as hydrostability, processability and separation.[10,15] Although significant progress has been made in this field, supramolecular polymeric elastomers crosslinked by MOPs have not yet been exploited.

Herein, we propose a chemical design of metal–organic polyhedra crosslinked supramolecular polymeric elastomers, referred to as ElastoMOPs. In particular, the ElastoMOPs consist of polytetramethylene glycol (PTMG) as the polymeric chains and Rh-based MOPs functionalized with different amounts of hydroxyl groups as the crosslinkers. The former serves as the soft domain of the ElastoMOPs, and the latter endows them with tunable network topologies and mechanical properties. As a result, the ElastoMOPs crosslinked by MOPs with more hydroxyl groups exhibited a larger tensile strength and storage modulus as well as longer relaxation time. The unique architecture and properties of ElastoMOPs inspired us to further exploit their potential applications in soft actuators.

The Rh-based MOPs with 12 Rh–Rh paddlewheel units and 24 ligands were utilized as the crosslinkers because of the good stability of their skeleton when the solvent molecules were removed from their cavities.[9b,16] The hydroxyl groups which can react with isocyanates were introduced onto the peripheries of the MOPs for crosslinking the polymeric chains as well as endowing the MOPs with solubility. Here, the principle of the structural design is maintaining the same amount of discrete MOP crosslinks in the polymeric matrix but varying the number of hydroxyl groups on each MOP, and thus tuning the network

School of Chemistry and Chemical Engineering, Frontiers Science Center for Transformative Molecules, Shanghai Jiao Tong University, Shanghai 200240, P. R. China. E-mail: xzyan@sjtu.edu.cn
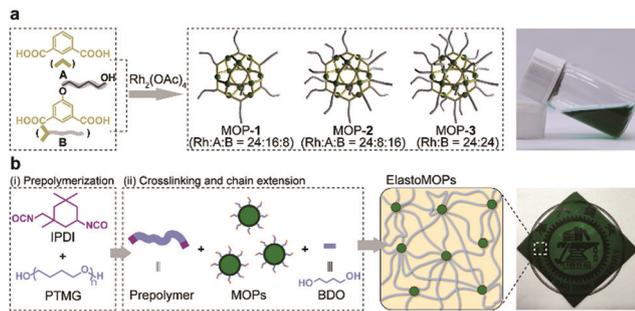
Scheme 1 (a) Self-assembly of the Rh-based MOPs with variable amounts of hydroxyl groups. The photograph shows the MOP-**3** solution in DMF. (b) Cartoon representation of the preparation of ElastoMOPs. The green film was made of ElastoMOP-**3**.

topologies of ElastoMOPs. To this end, MOP-**1**, MOP-**2**, and MOP-**3** with gradually increasing amounts of hydroxyl groups were synthesized by changing the molar ratio of isophthalic acid (**A**) and 5-(4-hydroxybutoxy)-1,3-benzenedicarboxylic acid (**B**) in the presence of $Rh_2(OAc)_4$ (Scheme 1a and Fig. S1, ESI†). The ^1H NMR spectra showed obvious upfield shifts of the aromatic protons, which indicated the formation of the carboxylate–Rh coordination bonds. Moreover, the broadening of the aromatic signals may originate from the restricted tumbling rotation of the coordination bonds (Fig. 1). In addition, the formation of the symmetric MOP structures was demonstrated by the simplicity of the spectra (Fig. S2, S4, and S6, ESI†). Then, we investigated the typical formation of the MOPs **1**–**3** by matrix-assisted laser desorption ionization/time of flight mass spectrometry (MALDI-TOF-MS). For MOP-**1** and MOP-**2**, because there was no clear force to regulate the self-assembly of the mixtures of **A** and **B**, statistical mixtures of the resultant MOPs were obtained as revealed by the peak distributions according to the MALDI-TOF-MS results (Fig. S3 and S5, ESI†). However, the main peaks at m/z = 7362.1 and 7815.2 confirmed the major
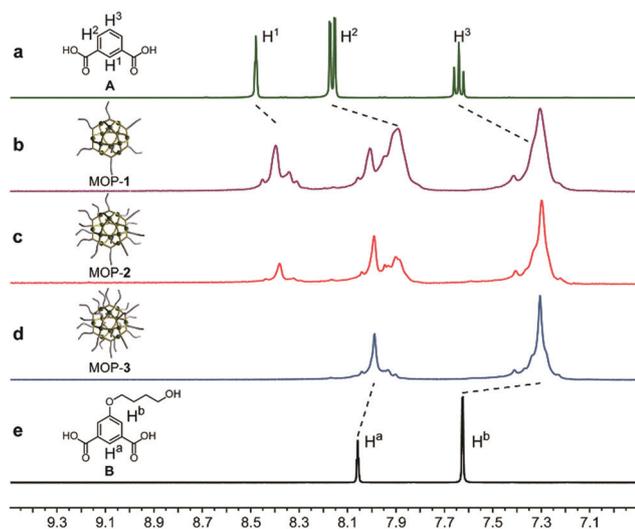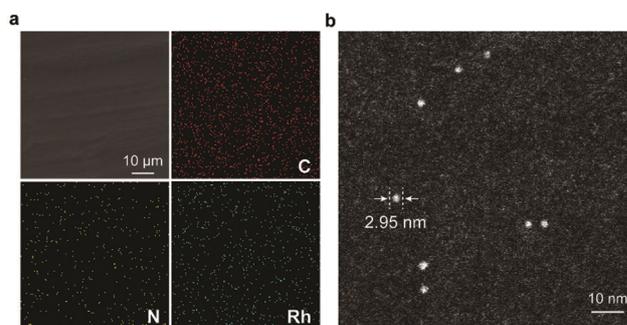
formulas of $[Rh_{24}A_{16}B_8 + H]^+$ + DCTB for MOP-**1** and $[Rh_{24}A_8B_{16} + H]^+$ + DCTB for MOP-**2**, respectively. For MOP-**3**, since only **B** participated in the coordination, a clean spectrum was observed with a single peak at m/z = 4259.1, corresponding to the formula of $[Rh_{24}B_{24} + 2H]^{2+}$. As such, we are able to prepare MOPs with controllable number of functionalized hydroxyl groups by means of coordination-driven co-assembly, which allows us to construct ElastoMOPs with tunable mechanical properties.

The synthetic route to the ElastoMOPs is illustrated in Scheme 1b. The prepolymer was obtained via the condensation reaction of isophorone diisocyanate (IPDI) and polytetramethylene glycol (PTMG, M_n = 1000 g mol^{-1}), followed by crosslinking with MOPs and chain extension with 1,4-butanediol (BDO). Additional BDO molecules were used to maintain NCO/OH = 1 for Elasto-MOPs **1**–**3**. Consequently, the final MOP contents of ElastoMOPs **1**–**3** were calculated to be 6.53, 7.15, and 7.78 wt%, respectively (Table S2, ESI†). The resultant ElastoMOPs can form a kind of transparent green film (Scheme 1b), which showed a characteristic absorption peak centered at λ_{max} = 599 nm, corresponding to the Rh–Rh paddlewheel units (Fig. S8, ESI†).[9b,14c] The thermal stabilities of the ElastoMOPs were measured by thermal gravimetric analysis (TGA). ElastoMOPs **1**–**3** exhibited almost the same thermal decomposition behaviors, wherein 5% weight loss occurred at about 280 °C, and the decomposition accelerated rapidly above this temperature (Fig. S9, ESI†). Furthermore, we selected ElastoMOP-**3** as a model system to investigate the morphologies of ElastoMOPs by scanning electron microscopy (SEM) and scanning transmission electron microscopy (STEM). The SEM image revealed a relatively smooth surface of the as-prepared ElastoMOP-**3** film (Fig. 2a). Moreover, the Rh distribution detected by energy-dispersive X-ray (EDX) mapping suggests that the MOPs were dispersed throughout the ElastoMOPs. In addition, since Rh has a significantly higher atomic number than the C and N atoms in the polymeric matrix, a high-angle annular dark-field STEM (HAADF-STEM) image was collected to obtain higher contrast morphology in detail. Therefore, we are able to observe the discrete MOP crosslinks in the matrix, which were shown as the bright particles with a diameter of ∼2.95 nm (Fig. 2b).

Besides their structural characteristics, we hypothesized that the increase in the number of hydroxyl groups on the MOPs would strengthen the mechanical properties of ElastoMOPs.

Fig. 1 Partial ^1H NMR spectra (DMSO-d_6, 298 K, 400 MHz) of (a) isophthalic acid (**A**), (b) MOP-**1**, (c) MOP-**2**, (d) MOP-**3**, and (e) 5-(4-hydroxybutoxy)-1,3-benzenedicarboxylic acid (**B**).


Fig. 2 (a) Top view of the SEM image and EDX mapping of ElastoMOP-**3**. (b) HAADF-STEM image of ElastoMOP-**3**.

Thus, we studied the mechanical behaviors of the three Elasto-MOPs. The tensile stress–strain profiles of the ElastoMOPs **1–3** are shown in Fig. 3a. The mechanical properties of the three Elasto-MOPs exhibited a continuously improving tendency with an increase in the number of hydroxyl groups on the MOP cross-linkers. Typical elastic deformations of the ElastoMOPs were observed with a strain of less than 20% with a linear behavior, while clear yield points appeared at an applied strain of around 60%. After this, the tensile stress increased with an increase of the applied strain contributed by the MOP crosslinks and finally reached the maximum tensile strength of each curve. Additionally, the curves of the ElastoMOPs **1–3** indicated that an increase in the number of hydroxyl groups on each crosslinker led to more polymeric chains anchored on the MOP cores, which further contributed to the improvement of the tensile strength. In order to evaluate their recovery properties, ElastoMOP-**3** was stretched and released successively for two cycles without interval. The tensile stress of the second stretch cycle was manifestly lower than that of the first cycle (Fig. 3b). However, after recovery of 1.5 h, the stress–strain curve overlapped well with the original one. These results suggested that ElastoMOPs are dynamic and mechanically adaptive.

To further estimate the dynamic features of ElastoMOPs, the step-strain relaxation experiments were performed (Fig. 3c). The ElastoMOPs were observed to relax the applied shear stress as the skeleton of the MOP crosslinks were broken to dissipate the energy, revealing the dynamic nature of the metal–ligand coordination bonds. However, the relaxation time of the Elas-toMOPs is highly dependent on the number of hydroxyl groups on MOP crosslinks (Fig. 3c). Moreover, the storage moduli of the ElastoMOPs were further investigated using a rheometer at a 5.0% strain amplitude and shearing frequency ranging from 0.01 to 100 rad s^{-1} at 40 °C (Fig. 3d). As the number of hydroxyl groups on MOPs crosslinks increased, the storage moduli (G')

of the ElastoMOPs enhanced accordingly, which were well consistent with the trend observed in the tensile test. In general, the introduction of crosslinks usually affects the mobility of the polymer backbones and therefore leads to variable rheological properties of the materials. As the number of hydroxyl groups on MOP crosslinks increased, more loops and crosslinking chains were formed, which resulted in the enhancement in the moduli of the ElastoMOPs (Fig. 3d and Fig. S10, ESI†). Therefore, the mechanical properties of the ElastoMOPs could be readily tuned through controlling the number of hydroxyl groups on the MOPs.

Notably, the incorporation of well-defined supramolecular architectures in polymeric materials not only endows them with unique structures and/or mechanical properties, but also plays a remarkable role in providing specific dynamic properties such as adaptivity and stimuli-responsiveness.[17] Similarly, MOPs with well-defined molecular structures should have the potential to endow ElastoMOPs with dynamic functions. Indeed, we found interesting stimulus-responsive bending behaviors of the Elasto-MOPs, like the curling of some plant vines driven by ambient moisture (Fig. 4a).[18] As shown in Fig. 4b, once the ElastoMOP-**3** specimen is exposed to an atmosphere of dichloromethane vapor (p = 47.4 kPa, 20 °C), the bending occurred quickly and reached the maximum bending angle of 81° in 4 seconds. When an air atmosphere was applied, the ElastoMOP-**3** recovered to the original shape for nearly 7 seconds (Fig. 4c and Movie S1, ESI†). The specimen could undergo several cycles of the bending-release process in 100 seconds but it cannot reach the maximum bending angle anymore in the following cycles due to the absorbed solvent molecules (Fig. S11, ESI†). Besides this, there are numerous examples of stimuli-responsive behaviors in biological systems. Inspired by the stimulus-driven unfolding and
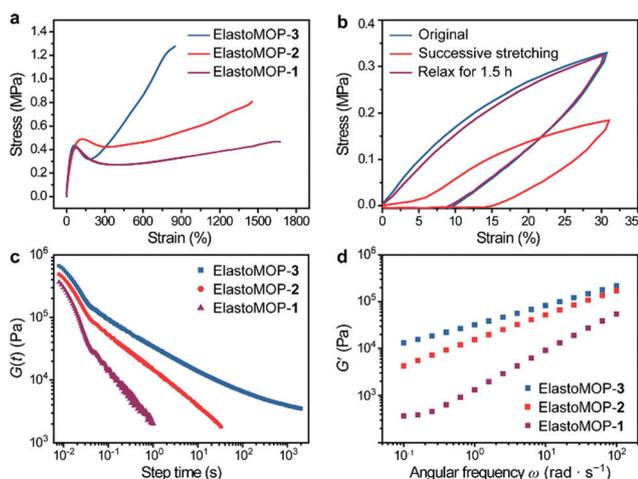
Fig. 3 (a) Tensile stress–strain curves of the ElastoMOPs **1–3**. Deformation rate: 100 mm min^{-1}. (b) Cyclic stress–strain tests of ElastoMOP-**3**. Deformation rate: 100 mm min^{-1}. (c) Step-strain (10%) relaxation curves of ElastoMOPs **1–3** at 40 °C. (d) Frequency sweeps from oscillatory rheometry of ElastoMOPs **1–3** at a 5.0% strain amplitude.
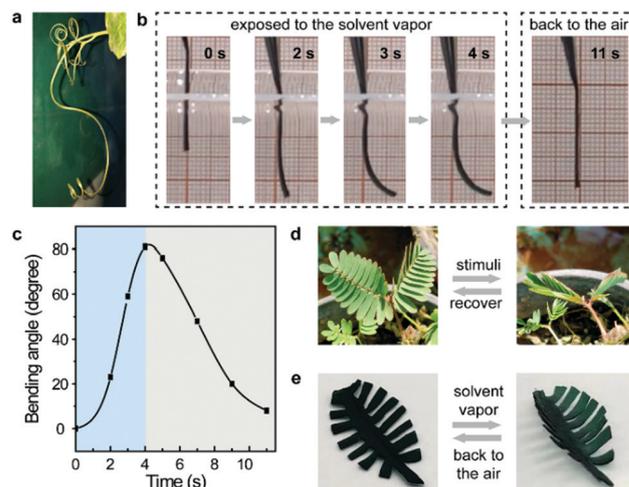
Fig. 4 (a) Photograph of the curled vines. (b) The actuator behaviors of the ElastoMOP-**3** film (2.0 × 30 × 0.34 mm) induced by dichloromethane vapor. (c) Plot of the bending angles against time for the ElastoMOP-**3** actuator shown in (b). (d) Photographs showing the unfolding and curling behaviors of the *mimosa*. (e) Demonstration that the leaf prepared from ElastoMOP-**3** can perform biomimetic movements upon exposure to dichloromethane vapor and then being transferred back to the air.

curling behaviors of the *mimosa* (Fig. 4d), ElastoMOP-**3** was formed into a *mimosa* leaf-like shape with a fixed petiole. The ElastoMOP leaf exhibited quick curling response upon exposure to dichloromethane vapor and recovered to its original state when moved back into air (Fig. 4e and Movie S2, ESI†). This biomimetic property may be attributed to the gradient difference in the extent of MOP crosslinks along the axis of the ElastoMOP-**3** films determined by the molding procedure, which led to the bending of the top surface inwards.[19] The molding procedure of the films was conducted on a PTFE plate at 90 °C, where the DMA solvent molecules continuously evaporated from the bottom to the top surface of the films, resulting in the formation of MOP crosslinks in a gradient distribution manner throughout its thickness. Therefore, upon exposure to the solvent vapor, inhomogeneous swelling led to the shape shifting of the ElastoMOP films. Such an interesting dynamic characteristic highlights potential applications of ElastoMOPs in smart materials.

In summary, we have fabricated and prepared metal–organic polyhedral cross-linked supramolecular polymeric elastomers (ElastoMOPs) which feature well-established MOP crosslinks and the consequent mechanical properties. In particular, the tensile strengths, storage moduli, and relaxation time of Elasto-MOPs can be readily tuned by varying the network topologies generated from controlling the number of hydroxyl groups on the MOPs. The unique structural characteristics and tunable mechanical properties of ElastoMOPs motivate us to further exploit their potential in the design of soft actuators. As such, we demonstrated a *mimosa*-inspired leak-like actuator made of the ElastoMOP film, which can undergo rapid bending in response to solvent vapor. Such a new structural design demonstrates an approach to adjust bulk properties of supramolecular materials hybridized with discrete MOPs. Therefore, ElastoMOPs will emerge as promising platforms for the exploitation and applications of mechanically adaptive supramolecular materials.

Conflicts of interest

There are no conflicts to declare.

Notes and references

1 (*a*) A. J. Ridley and A. Hall, *Cell*, 1992, **70**, 389–399; (*b*) X. Yan, F. Wang, B. Zheng and F. Huang, *Chem. Soc. Rev.*, 2012, **41**, 6042–6065.
2 S. Mena-Hernando and E. M. Pérez, *Chem. Soc. Rev.*, 2019, **48**, 5016–5032.
3 (*a*) S. Datta, M. L. Saha and P. J. Stang, *Acc. Chem. Res.*, 2018, **51**, 2047–2063; (*b*) Y. Han, Y. Tian, Z. Li and F. Wang, *Chem. Soc. Rev.*, 2018, **47**, 5165–5176.
4 D.-W. Zhang, X. Zhao and Z.-T. Li, *Acc. Chem. Res.*, 2014, **47**, 1961–1970.
5 (*a*) C.-H. Li, C. Wang, C. Keplinger, J.-L. Zuo, L. Jin, Y. Sun, P. Zheng, Y. Cao, F. Lissel, C. Linder, X.-Z. You and Z. Bao, *Nat. Chem.*, 2016, **8**, 618–624; (*b*) X. Yan, Z. Liu, Q. Zhang, J. Lopez, H. Wang, H.-C. Wu, S. Niu, H. Yan, S. Wang, T. Lei, J. Li, D. Qi, P. Huang, J. Huang, Y. Zhang, Y. Wang, G. Li, J. B. H. Tok, X. Chen and Z. Bao, *J. Am. Chem. Soc.*, 2018, **140**, 5280–5289.
6 (*a*) X.-Q. Wang, W. Wang, W.-J. Li, L.-J. Chen, R. Yao, G.-Q. Yin, Y.-X. Wang, Y. Zhang, J. Huang, H. Tan, Y. Yu, X. Li, L. Xu and H.-B. Yang, *Nat. Commun.*, 2018, **9**, 3190; (*b*) S. Wang, Z. Xu, T. Wang, T. Xiao, X.-Y. Hu, Y.-Z. Shen and L. Wang, *Nat. Commun.*, 2018, **9**, 1737; (*c*) Z. Gao, Y. Han and F. Wang, *Nat. Commun.*, 2018, **9**, 3977.
7 (*a*) M. Arunachalam and H. W. Gibson, *Prog. Polym. Sci.*, 2014, **39**, 1043–1073; (*b*) T. L. Price and H. W. Gibson, *J. Am. Chem. Soc.*, 2018, **140**, 4455–4465; (*c*) K. Liu, Y. Jiang, Z. Bao and X. Yan, *CCS Chem.*, 2019, **1**, 431–447.
8 R. Chakrabarty, P. S. Mukherjee and P. J. Stang, *Chem. Rev.*, 2011, **111**, 6810–6918.
9 (*a*) X. Yan, S. Li, J. B. Pollock, T. R. Cook, J. Chen, Y. Zhang, X. Ji, Y. Yu, F. Huang and P. J. Stang, *Proc. Natl. Acad. Sci. U. S. A.*, 2013, **110**, 15585–15590; (*b*) A. Carné-Sánchez, J. Albalad, T. Grancha, I. Imaz, J. Juanhuix, P. Larpent, S. Furukawa and D. Maspoch, *J. Am. Chem. Soc.*, 2019, **141**, 4094–4102.
10 J. Liu, W. Duan, J. Song, X. Guo, Z. Wang, X. Shi, J. Liang, J. Wang, P. Cheng, Y. Chen, M. J. Zaworotko and Z. Zhang, *J. Am. Chem. Soc.*, 2019, **141**, 12064–12070.
11 L.-J. Chen and H.-B. Yang, *Acc. Chem. Res.*, 2018, **51**, 2699–2710.
12 N. Hosono and S. Kitagawa, *Acc. Chem. Res.*, 2018, **51**, 2437–2446.
13 (*a*) C. Lu, M. Zhang, D. Tang, X. Yan, Z. Zhang, Z. Zhou, B. Song, H. Wang, X. Li, S. Yin, H. Sepehrpour and P. J. Stang, *J. Am. Chem. Soc.*, 2018, **140**, 7674–7680; (*b*) G.-F. Huo, X. Shi, Q. Tu, Y.-X. Hu, G.-Y. Wu, G.-Q. Yin, X. Li, L. Xu, H.-M. Ding and H.-B. Yang, *J. Am. Chem. Soc.*, 2019, **141**, 16014–16023; (*c*) W. Zheng, W. Wang, S.-T. Jiang, G. Yang, Z. Li, X.-Q. Wang, G.-Q. Yin, Y. Zhang, H. Tan, X. Li, H. Ding, G. Chen and H.-B. Yang, *J. Am. Chem. Soc.*, 2019, **141**, 583–591.
14 (*a*) N. Hosono, M. Gochomori, R. Matsuda, H. Sato and S. Kitagawa, *J. Am. Chem. Soc.*, 2016, **138**, 6525–6531; (*b*) A. V. Zhukhovitskiy, M. Zhong, E. G. Keeler, V. K. Michaelis, J. E. P. Sun, M. J. A. Hore, D. J. Pochan, R. G. Griffin, A. P. Willard and J. A. Johnson, *Nat. Chem.*, 2016, **8**, 33–41; (*c*) A. Carné-Sánchez, G. A. Craig, P. Larpent, T. Hirose, M. Higuchi, S. Kitagawa, K. Matsuda, K. Urayama and S. Furukawa, *Nat. Commun.*, 2018, **9**, 2506; (*d*) Y. Gu, E. A. Alt, H. Wang, X. Li, A. P. Willard and J. A. Johnson, *Nature*, 2018, **560**, 65–69.
15 X.-Y. Xie, F. Wu, X. Liu, W.-Q. Tao, Y. Jiang, X.-Q. Liu and L.-B. Sun, *Chem. Commun.*, 2019, **55**, 6177–6180.
16 S. Furukawa, N. Horike, M. Kondo, Y. Hijikata, A. Carné-Sánchez, P. Larpent, N. Louvain, S. Diring, H. Sato, R. Matsuda, R. Kawano and S. Kitagawa, *Inorg. Chem.*, 2016, **55**, 10843–10846.
17 (*a*) B. Zhu, M. Noack, R. Merindol, C. Barner-Kowollik and A. Walther, *Nano Lett.*, 2016, **16**, 5176–5182; (*b*) J. Troyano, A. Carné-Sánchez, J. Pérez-Carvajal, L. León-Reina, I. Imaz, A. Cabeza and D. Maspoch, *Angew. Chem., Int. Ed.*, 2018, **57**, 15420–15424; (*c*) J. Troyano, A. Carné-Sánchez and D. Maspoch, *Adv. Mater.*, 2019, **31**, 1808235.
18 A. Rafsanjani, V. Brulé, T. L. Western and D. Pasini, *Sci. Rep.*, 2015, **5**, 8064.
19 (*a*) T. S. Kelby, M. Wang and W. T. S. Huck, *Adv. Funct. Mater.*, 2011, **21**, 652–657; (*b*) L. Montero de Espinosa, W. Meesorn, D. Moatsou and C. Weder, *Chem. Rev.*, 2017, **117**, 12851–12892.